

# Accelerated Bayesian SED Modeling using Amortized Neural Posterior Estimation

CHANGHOON HAHN<sup>1,\*</sup> AND PETER MELCHIOR<sup>1</sup>

<sup>1</sup>*Department of Astrophysical Sciences, Princeton University, Peyton Hall, Princeton NJ 08544, USA*

## ABSTRACT

State-of-the-art spectral energy distribution (SED) analyses use a Bayesian framework to infer the physical properties of galaxies from observed photometry and spectra. They require sampling a high dimensional space of SED model parameters and, thus, take  $> 10 - 100$  CPU hours per galaxy. Current models are not computationally feasible for analyzing the *millions* of galaxies that will be observed by upcoming galaxy surveys (*e.g.* DESI, PFS, Rubin, James Webb, and Roman). In this work, we present an alternative *scalable* approach for rigorous Bayesian inference using Amortized Neural Posterior Estimation (ANPE). ANPE is a simulation-based inference method that exploits neural network models to estimate the posterior probability distribution over the full range of observations. It requires no additional model evaluations to estimate the posterior after training. To demonstrate the advantages of an ANPE approach, we present SEDFLOW, an SED modeling method that uses ANPE with the recent ? SED model, and apply it to optical photometry. Once trained, deriving the posterior of galaxy properties with SEDFLOW takes  $\sim 1$  *second per galaxy*. Furthermore, we validate SEDFLOW using posteriors derived from standard Markov Chain Monte Carlo (MCMC) sampling and synthetic observations, with known true parameter values. The SEDFLOW posteriors are in excellent agreement with both the MCMC estimates and the true posteriors. We therefore conclude that using ANPE we derive accurate posteriors  $> 10,000\times$  faster than standard SED modeling methods. Lastly, we apply SEDFLOW to 33,887 galaxies in the NASA-Sloan Atlas and publicly release the posteriors of galaxy properties for every galaxy.

*Keywords:* galaxies: evolution – galaxies: statistics

## 1. INTRODUCTION

Over the past few decades, observations from large galaxy surveys such as the Sloan Digital Sky Survey (SDSS; York et al. 2000), DEEP2 (Davis et al. 2003), COSMOS and zCOSMOS (Scoville et al. 2007; Lilly et al. 2007), and GAMA (Baldry et al. 2018) have transformed our understanding of how galaxies form and evolve. The building blocks of our physical insight into galaxies are their physical properties measured from these observations: *e.g.* stellar mass ( $M_*$ ), star formation rate

\* changhoon.hahn@princeton.edu.com

(SFR), metallicity ( $Z$ ), and age ( $t_{\text{age}}$ ). The primary way for measuring these galaxy properties is by analyzing their spectral energy distribution (SED).

All of the physical processes in a galaxy leave an imprint on its SED. For instance, the SED over the ultraviolet to infrared wavelengths is primarily composed of light from the galaxy’s stellar populations and, thus, encodes the galaxy’s star formation and chemical enrichment histories. How some of this stellar light is reprocessed reflects the gas and dust content of the galaxy’s interstellar medium. The goal of SED modeling is to extract the detailed physical properties of galaxies that are encoded in observed SEDs. There are three key components to SED modeling: the observations, a physical SED model, and a statistical inference framework for deriving physical properties from comparisons between the observations and models.

Current SED models are based on stellar population synthesis (SPS). Broadly speaking, they model the SED of a galaxy as a composite stellar population constructed from isochrones, stellar spectra, an initial mass function (IMF), a star formation and chemical evolution history, and dust attenuation (*e.g.* Bruzual & Charlot 2003; Maraston 2005; Conroy et al. 2009). Some models also include dust and nebular emissions as well as emissions from active galactic nuclei (*e.g.* Johnson et al. 2021). For a comprehensive review on SPS and SED modeling, we refer readers to Walcher et al. (2011) and Conroy (2013).

In this work, we focus on the third component of SED modeling: the statistical framework for comparing the physical SED models to observations and inferring galaxy properties. State-of-the-art SED modeling use a Bayesian inference framework. This approach has a number of key advantages over maximum-likelihood approaches (*e.g.* Cid Fernandes et al. 2005; Tojeiro et al. 2007; Koleva et al. 2008) that were often used in the past. In Bayesian inference, the goal is to estimate  $p(\theta | \mathbf{x})$ , the probability distribution of parameters  $\theta$ , in our case galaxy properties, given observation  $\mathbf{x}$ . Inferring  $p(\theta | \mathbf{x})$  provides an accurate estimate of parameter uncertainties and any degeneracies among them that can then be propagated for more accurate statistical analyses. The Bayesian framework also enables marginalization over nuisance parameters, which is necessary to model the effects of observational systematics (*e.g.* flux calibration). In principle, Bayesian inference also allows us to exploit informative priors based on previous observations to derive more precise constraints on galaxy properties.

In practice, current Bayesian methods use Markov Chain Monte Carlo (MCMC) sampling techniques to explore and estimate the posterior (Acquaviva et al. 2011; Chevallard & Charlot 2016; Leja et al. 2017; Carnall et al. 2018). MCMC sampling enables more accurate posterior estimation and addresses the curse of dimensionality that restricts grid-based techniques often used in the past (Kauffmann et al. 2003; Burgarella et al. 2005; Salim et al. 2007; da Cunha et al. 2008). Grid-based techniques require SED models to be pre-computed over a grid in parameter space. Hence, as the dimensionality of model parameters increases for more sophisticated models, they require exponentially large number of model evaluations. Meanwhile for MCMC, the number of evaluations scales roughly linearly with the number of parameters. In Johnson et al. (2021), for instance, they use MCMC to sample a 16-dimensional parameter space.

Despite their advantages, current Bayesian SED modeling methods are *not scalable* as upcoming galaxy surveys will observe an unprecedented number of galaxies. The Dark Energy Spectroscopic Survey (DESI; Collaboration et al. 2016), the Prime Focus Spectrograph (PFS; Takada et al. 2014), Rubin observatory (Ivezić et al. 2019), and Roman Space Telescope (Spergel et al. 2015) will all observe *millions* of galaxy SEDs. Meanwhile, current SED modeling takes 10-100 CPU hours per galaxy (e.g. Tacchella et al. 2021). With current methods, inferring galaxy properties from rigorous Bayesian SED modeling for upcoming surveys would require *billions* of CPU hours.

The computational challenge is further exacerbated by additional factors. First, more accurate and sophisticated SED models require additional parameters. For instance, modeling additional physical processes such as nebular emission requires additional parameters. Accurately incorporating observational effects also requires extra parameters. As the dimensionality expands, conventional sampling techniques are less efficient. Second, it has recently come to light that the prior, used to evaluate the posterior, can significantly impact the inferred galaxy properties (Carnall et al. 2017; Leja et al. 2017; ?). This is a consequence of the fact that galaxy properties are not input SED model parameters but rather derived quantities (see Appendix of ?). Hence, deriving robust galaxy properties requires validating the properties using different priors and investigating their impact. For MCMC-based methods, posteriors would need to be re-evaluated from scratch for each prior. Lastly, current SED modeling make strong theoretical assumptions. They make explicit choices for stellar spectral library and initial mass function, even though there is no consensus. Relaxing these assumptions would involve flexibly parameterizing the uncertainties and variations as additional parameters in SED models (Conroy et al. 2009; ?) or deriving galaxy properties for multiple sets of assumptions. Both options increase the computational costs of current SED modeling.

Rigorous Bayesian inference, however, does not require MCMC sampling. Simulation-based inference (SBI; also known as “likelihood-free inference”) is a rapidly developing class of inference methods that offers better alternatives for many applications (see Cranmer et al. 2020, and reference therein). Many SBI methods leverage the latest developments in statistics and Machine Learning for more efficient posterior estimation (Papamakarios et al. 2017; Alsing et al. 2019; Hahn et al. 2019; Dax et al. 2021; Huppenkothen & Bachetti 2021; Zhang et al. 2021). One such SBI technique optimal for scalable Bayesian inference is Amortized Neural Posterior Estimation (ANPE).

ANPE utilizes a density estimation approach to SBI. Instead of using MCMC to sample the posterior,  $p(\theta | \mathbf{x}_i)$ , of a single galaxy,  $i$ , ANPE uses neural density estimators (NDE) and training data to estimate  $p(\theta | \mathbf{x})$  over the full space of observables  $\mathbf{x}$ . NDEs are density models parameterized by neural networks that estimate density/probability distributions. The training data are  $\{(\theta_i, \mathbf{x}'_i)\}$  pairs. In our application,  $\theta$  is the SED model parameters, sampled from a prior, and  $\mathbf{x}'_i$  are synthetic observables, such as photometry, forward modeled using the SED model. Once the NDE is trained, generating the posterior requires no additional model evaluations and only requires plugging in the observation  $\mathbf{x}_i$ .

ANPE addresses one of the major drawbacks of MCMC: SED model evaluations used for one galaxy cannot be used for another. This is why MCMC sampling has to be performed on every galaxy. In ANPE, models evaluations are only used to construct the training data of the NDE.

Although the training set typically requires more evaluations than for a single MCMC posterior, no additional evaluations are necessary after training. Hence, the computational cost is *amortized* and only a minuscule fraction of the cost of performing MCMC to analyze a large set of observations. ANPE has recently been applied to a wide range of applications in physics and astronomy with remarkable success (Stein et al. 2020; Wong et al. 2020; Dax et al. 2021; Zhang et al. 2021).

In this work, we present SEDFLOW, a method that applies ANPE to Bayesian galaxy SED modeling using the recent ? SED model. We demonstrate that we can derive accurate posteriors with SEDFLOW and make Bayesian SED modeling fully scalable for the millions of galaxies that will be observed by upcoming surveys. As further demonstration, we apply ANPE to analyze optical photometry of  $\sim 33,000$  galaxies in the NASA-Sloan Atlas (NSA<sup>1</sup>). We begin in Section 2 by describing SBI using ANPE. We then describe the NSA observations in Section 3. Afterwards, we present how we design and train SEDFLOW in Section 4. We validate the accuracy of the posteriors from SEDFLOW in Section 5 and discuss the implication of our results and future steps in Section 5.1.

## 2. SIMULATION-BASED INFERENCE

The ultimate goal of Bayesian SED modeling, and probabilistic inference more broadly, is to infer the posterior probability distributions of galaxy properties,  $\theta$ , given observations,  $\mathbf{x}_{\text{obs}} \sim p(\theta | \mathbf{x}_{\text{obs}})$ . For a specific  $\theta$  and  $\mathbf{x}$ , we can evaluate the posterior using Bayes’ rule,  $p(\theta | \mathbf{x}_{\text{obs}}) \propto p(\theta) p(\mathbf{x}_{\text{obs}} | \theta)$ .  $p(\theta)$  is the prior distribution, which we specify, and  $p(\mathbf{x}_{\text{obs}} | \theta)$  is the likelihood, which is *typically* evaluated using a surrogate Gaussian functional form:

$$\ln p(\mathbf{x}_{\text{obs}} | \theta) = -\frac{1}{2}(\mathbf{x}_{\text{obs}} - m(\theta))^T \mathbf{C}^{-1}(\mathbf{x}_{\text{obs}} - m(\theta)). \quad (1)$$

$m(\theta)$  is the theoretical model, in our case a galaxy SED model from SPS.  $\mathbf{C}$  is the covariance matrix of the observations. In practice, off-diagonal terms are often ignored and measured uncertainties are used as estimates of the diagonal terms.

In the standard approach, the full posterior distribution is estimated by exploring the posterior with a sampling technique such as Markov Chain Monte Carlo (MCMC; *e.g.* Carnall et al. 2018; Leja et al. 2019b; Tacchella et al. 2021). These sampling techniques are essential for the efficient exploration given the relatively high dimensionality of SED model parameter space. Even advanced techniques, however, are subject to major limitations. For instance, MCMC can struggle to accurately estimate multimodal and degenerate posteriors. Many techniques also require significant hand-tuning. More importantly, despite their efficiency, these techniques require on the order of a *million* SED model evaluations to derive a posterior — this can take  $\sim 10 - 100$  of CPU hours per galaxy. Analyzing the tens of millions of spectra or billions of photometry from upcoming surveys (*e.g.* DESI, PFS, Rubin, JWST, Roman) with these approaches would thus require *billions of CPU hours*.

Simulation-based inference (SBI; also known as “likelihood-free” inference) offers a more scalable approach to Bayesian SED modeling. At its core, SBI involves any method that uses a forward model of the observed data to directly estimate the posterior —  $p(\theta | \mathbf{x})$ , the likelihood —  $p(\mathbf{x} | \theta)$ , or the

<sup>1</sup> <http://www.nsatlas.org/>

joint distribution of the parameters and data —  $p(\theta, \mathbf{x})$ . SBI has already been successfully applied to a number of Bayesian parameter inference problems in astronomy (*e.g.* Cameron & Pettitt 2012; Weyant et al. 2013; Hahn et al. 2017; Kacprzak et al. 2018; Alsing et al. 2018; Wong et al. 2020; Huppenkothen & Bachetti 2021; Zhang et al. 2021), and in physics (*e.g.* Brehmer et al. 2019; Cranmer et al. 2020).

One simple and pedagogical example of SBI is Approximate Bayesian Computation (ABC; Rubin 1984; Pritchard et al. 1999; Beaumont et al. 2002), which uses a rejection sampling framework to estimate the posterior. First, parameter values are sampled from the prior:  $\theta' \sim p(\theta)$ . The forward model,  $F$ , is then run on  $\theta'$  to generate simulated data  $F(\theta') = \mathbf{x}'$ . If the simulated  $\mathbf{x}'$  is ‘close’ to the observed  $\mathbf{x}_{\text{obs}}$ , usually based on a threshold on some distance criterion  $\rho(\mathbf{x}', \mathbf{x}_{\text{obs}}) < \epsilon$ ,  $\theta'$  is kept. Otherwise,  $\theta'$  is rejected. This process is repeated until there are enough samples to estimate the posterior. The estimated posterior from ABC can be written as  $p(\theta | \rho(F(\theta), \mathbf{x}_{\text{obs}}) < \epsilon)$ . In the case where  $\epsilon \rightarrow 0$ , the conditional statement is equivalent to the condition  $F(\theta) = \mathbf{x}_{\text{obs}}$ ; thus, the estimated ABC posterior is equivalent to the true posterior:  $p(\theta | \rho(F(\theta), \mathbf{x}_{\text{obs}}) < \epsilon \rightarrow 0) \equiv p(\theta | \mathbf{x}_{\text{obs}})$ .

ABC produces unbiased estimates of the posterior and only requires a forward model of the observed data. It makes no assumptions on the likelihood and, therefore, relaxes the assumptions that go into surrogate likelihood methods. Nevertheless, ABC is based on rejection sampling and thus requires comparable number of model evaluations as standard MCMC sampling based techniques. ABC is only the simplest SBI method; new SBI methods can infer posteriors with much fewer model evaluations. Density estimation-based SBI methods (*e.g.* Papamakarios et al. 2017; Alsing et al. 2018; Hahn et al. 2019; Greenberg et al. 2019; Tejero-Cantero et al. 2020), for instance, use model evaluations to fit the  $p(\theta | \mathbf{x}_{\text{obs}})$ ,  $p(\mathbf{x} | \theta)$ , or  $p(\theta, \mathbf{x})$  probability distributions. They can exploit recent advances in neural density estimation (NDE) that increasingly enable high-fidelity density estimation with fewer samples of the distribution. For instance, the NDE in Papamakarios et al. (2017) accurately estimates the  $28 \times 28 = 784$ -dimensional distribution of the MNIST dataset<sup>2</sup> with only tens of thousands of samples.

### 2.1. Amortized Neural Posterior Estimation

Density estimation SBI provides a critical advantage over MCMC sampling-based inference methods — it enables *amortized inference*. For SED modeling using MCMC, each galaxy requires  $>10^5$  model evaluations to accurately estimate  $p(\theta | \mathbf{x}_{\text{obs}})$ . Moreover, model evaluations for calculating the posterior of one galaxy cannot be used for another. For large galaxy surveys with  $>10^6$  galaxies (*e.g.* SDSS, Ahumada et al. 2020) this would require  $>100$  billion model evaluations. Upcoming galaxy surveys will observe orders of magnitude more galaxies (*e.g.* DESI, PFS, Rubin, Roman). Bayesian SED modeling with MCMC sampling for these large galaxy surveys is utterly *computationally infeasible*.

On the other hand, if we use density estimation SBI for SED modeling, we do not require a large number of model evaluations for each galaxy. An initial set of model evaluations ( $\sim 10^6$ ) is necessary to train an NDE to accurately estimate  $\hat{p}(\theta | \mathbf{x}_{\text{obs}})$  — *i.e.* Amortized Neural Posterior

<sup>2</sup> <http://yann.lecun.com/exdb/mnist/>



Estimation (ANPE). Once trained,  $\hat{p}(\theta | \mathbf{x}_{\text{obs}})$  is estimated over the full  $\theta$  and  $\mathbf{x}_{\text{obs}}$ -space so we can sample  $\hat{p}(\theta | \mathbf{x}_{\text{obs},i})$  for each galaxy with minimal computational cost. The inference is amortized and no additional model evaluations are needed to generate the posterior for each galaxy. In total, SED modeling with ANPE for  $>10^6$  galaxies requires the same number of model evaluations as analyzing tens of galaxies using MCMC.

ANPE has recently been applied to a broad range of astronomical applications from analyzing gravitational waves (*e.g.* Wong et al. 2020; Dax et al. 2021) to binary microlensing lensing (Zhang et al. 2021). They primarily use a class of NDE called normalizing flows (Tabak & Vanden-Eijnden 2010; Tabak & Turner 2013). Normalizing flow models use an invertible bijective transformation,  $f$ , to map a complex target distribution to a simple base distribution,  $\pi(z)$ , that is fast to evaluate. For ANPE, the target distribution is  $p(\theta | \mathbf{x})$  and the  $\pi(z)$  is typically a simple multivariate Gaussian, or mixture of Gaussians.

The transformation  $f : z \rightarrow \theta$  must be invertible and have a tractable Jacobian. This is so that we can evaluate the target distribution from  $\pi(z)$  using change of variable:

$$p(\theta | \mathbf{x}) = \pi(z) \left| \det \left( \frac{\partial f^{-1}}{\partial \theta} \right) \right|. \quad (2)$$

Since the base distribution is easy to evaluate, we can also easily evaluate the target distribution. A neural network is trained to obtain  $f$ . The network typically consists of a series of simple transforms (*e.g.* shift and scale transforms) that are each invertible and whose Jacobians are easily calculated. By stringing together many such transforms,  $f$  provides an extremely flexible mapping from the base distribution.

Many different normalizing flow models are now available in the literature (*e.g.* Germain et al. 2015; Durkan et al. 2019). In this work, we use Masked Autoregressive Flow (MAF; Papamakarios et al. 2017). The autoregressive design (Uria et al. 2016) of MAF is particularly well-suited for modeling conditional probability distributions such as the posterior. Autoregressive models exploit chain rule to expand a joint probability of a set of random variables as products of one-dimensional conditional probabilities:  $p(x) = \prod_i p(x_i | x_{1:i-1})$ . They then use neural networks to describe each conditional probability,  $p(x_i | x_{1:i-1})$ . In this context, we can add a conditional variable  $y$  on both sides of the equation,  $p(x | y) = \prod_i p(x_i | x_{1:i-1}, y)$ , so that the autoregressive model describes a conditional probability  $p(x | y)$ . One drawback of autoregressive models is their sensitivity to the ordering of the variables. Masked Autoencoder for Distribution Estimation (MADE; Germain et al. 2015) models address this limitation by dropping out connections of a fully-connected autoencoder using weight matrices with binary masks. This ensures that the MADE model is autoregressive and can be efficiently calculated. A MAF model is built by stacking multiple MADE models. Hence, it has the autoregressive structure of MADE but with more flexibility to describe complex probability distributions. In practice, we use the MAF implementation in the `sbi` Python package<sup>3</sup> (Greenberg et al. 2019; Tejero-Cantero et al. 2020).

<sup>3</sup> <https://github.com/mackelab/sbi/>

### 3. NASA-SLOAN ATLAS

As a demonstration of its speed and accuracy, we apply SEDFLOW to optical photometry from the NASA-Sloan Atlas<sup>4</sup> (NSA). The NSA catalog is a re-reduction of SDSS DR8 (Aihara et al. 2011) that includes an improved background subtraction (Blanton et al. 2011). We use SDSS photometry in the  $u$ ,  $g$ ,  $r$ ,  $i$ , and  $z$  bands, which are corrected for galactic extinction using Schlegel et al. (1998). To ensure that the galaxy sample is not contaminated, we impose a number of additional quality cuts by excluding:

- objects where the centroiding algorithm reports the position of the peak pixel in a given band as the centroid. The SDSS photometric pipeline can struggle to accurately define the center of objects near the edge or at low signal-to-noise, so these cases are often associated with spurious objects.
- objects that have pixels that were not checked for peaks by the deblender.
- objects where more than 20% of point-spread function (PSF) flux is interpolated over as well as objects where the interpolation affected many pixels and the PSF flux error is inaccurate. The SDSS pipeline interpolates over pixels classified as bad (*e.g.* cosmic ray).
- objects where the interpolated pixels fall within 3 pixels of their center and they contain a cosmic ray that was interpolated over.
- objects that were not detected at  $\geq 5\sigma$  in the original frame, that contain saturated pixels, or where their radial profile could not be extracted.

By excluding these objects, we avoid complications from artifacts in the photometry that we do not model. For additional details on the quality flags, we refer readers to the SDSS documentation<sup>5</sup>. After the quality cuts, we have a total of 33,887 galaxies in our NSA sample.

### 4. SEDFLOW

In this section, we present SEDFLOW, which applies ANPE to SED modeling for a scalable and accelerated approach. For our SED model, we use the state-of-the-art PROVABGS model from ?. Although many SED models have been recently used in the literature (*e.g.* BAGPIPES, Carnall et al. 2018; PROSPECTOR, Leja et al. 2017; Johnson et al. 2021), we choose PROVABGS because it will be used to analyze >10 million galaxy spectrophotometry measured by the DESI Bright Galaxy Survey (Ruiz-Macias et al. 2021; ?). Below, we describe the PROVABGS model, the construction of the SEDFLOW training data using PROVABGS, and the training procedure for SEDFLOW.

#### 4.1. SED Modeling: PROVABGS

We use the state-of-the-art SPS model of the PROVABGS (Hahn et al. 2022). The SED of a galaxy is modeled as a composite of stellar populations defined by stellar evolution theory (in the

<sup>4</sup> <http://nsatlas.org/>

<sup>5</sup> [https://www.sdss.org/dr16/algorithms/flags\\_detail](https://www.sdss.org/dr16/algorithms/flags_detail)

form of isochrones, stellar spectral libraries, and an initial mass function) and its star formation and chemical enrichment histories (SFH and ZH), attenuated by dust (see Walcher et al. 2011; Conroy 2013, for a review). The PROVABGS model, in particular, utilizes a non-parametric SFH with a starburst, a non-parametric ZH that varies with time, and a flexible dust attenuation prescription.

The SFH has two components: one based on non-negative matrix factorization (NMF) bases and the other, a starburst component. The SFH contribution from the NMF component is a linear combination of four NMF SFH basis functions, derived from performing NMF (Lee & Seung 1999; Cichocki & Phan 2009; Févotte & Idier 2011) on SFHs of galaxies in the Illustris cosmological hydrodynamical simulations (Vogelsberger et al. 2014; Genel et al. 2014; Nelson et al. 2015). The NMF SFH prescription provides a compact and flexible representation of the SFH. The second starburst component consists of a single stellar population (SSP) and adds stochasticity to the SFH.

The ZH is similarly defined using two NMF bases derived from Illustris. This ZH prescription enables us to flexibly model a wide range of ZHs and unlike most SED models, it does not assume constant metallicity over time, which can significantly bias inferred galaxy properties (Thorne et al. 2021). The stellar evolution theory is based on Flexible Stellar Population Synthesis (FSPS; Conroy et al. 2009; Conroy & Gunn 2010) with the MIST isochrones (Paxton et al. 2011, 2013, 2015; Choi et al. 2016; Dotter 2016), the Chabrier (2003) initial mass function (IMF), and a combination of the MILES (Sánchez-Blázquez et al. 2006) and BaSeL (Lejeune et al. 1997, 1998; Westera et al. 2002) libraries. The SFH and ZH are binned into 43 logarithmically-space time bin and SSPs are evaluated at each time bin using FSPS. The SSPs are summed up to get the unattenuated rest-frame galaxy SED.

Lastly, PROVABGS attenuates the light from the composite stellar population using the two component Charlot & Fall (2000) dust attenuation model with diffuse-dust (ISM) and birth cloud (BC) components. All SSPs are attenuated by the diffuse dust using the Kriek & Conroy (2013) attenuation curve. Then, the BC component provides extra dust attenuation on SSPs younger than 100 Myr with young stars that are embedded in molecular clouds and HII regions. In total the PROVABGS SED model has 12 free parameters: stellar mass ( $M_*$ ), six SFH parameters ( $\beta_1, \beta_2, \beta_3, \beta_4, t_{\text{burst}}, f_{\text{burst}}$ ), two ZH parameters ( $\gamma_1, \gamma_2$ ), and three dust attenuation parameters ( $\tau_{\text{BC}}, \tau_{\text{ISM}}, n_{\text{dust}}$ ). Each PROVABGS model evaluation takes  $\sim 340$  ms.

#### 4.2. Training Data

In this section, we describe how to we construct the training data for SEDFLOW using the PROVABGS SED model. First, we sample  $N_{\text{train}}$  SED model parameters from a prior:  $\theta' \sim p(\theta)$ . We use the same priors as Hahn et al. (2022): uniform priors over  $M_*, t_{\text{burst}}, f_{\text{burst}}, \gamma_1, \gamma_2, \tau_{\text{BC}}, \tau_{\text{ISM}}, n_{\text{dust}}$  with broad conservative ranges and Dirichlet prior over  $\beta_1, \beta_2, \beta_3, \beta_4$ , chosen to normalize the NMF SFH. For each  $\theta'$ , we also uniformly sample a redshift within the range of the NSA:  $z' \sim \mathcal{U}(0., 0.2)$ . Next, we forward model mock observables — NSA optical photometry (Section 3). We calculate the rest-frame galaxy SED from PROVABGS and redshift it:  $F(\lambda; \theta', z)$ . Afterwards, we convolve  $F$  with optical broadband filters,  $R_X$ , to generate noiseless photometric fluxes:

$$f_X(\theta', z') = \int F(\lambda; \theta', z') R_X(\lambda) d\lambda \quad (3)$$





**Figure 1.** Joint distribution of SED model parameters, redshift, photometric magnitudes, and uncertainties of the data used to train SEDFLOW. We plot only a subset of the parameters ( $\log M_*$ ,  $\beta_1$ ) and photometric bands for clarity. The training data was constructed by sampling SED model parameter values from the prior and forward modeling optical photometry using the PROVABGS and noise models (Section 4). For comparison, we present the distribution of redshift, magnitudes, and uncertainties for galaxies in the NSA catalog (blue). *The training set fully encompasses the observations; thus, SEDFLOW can be used to infer the posterior for all NSA galaxies.*

The next step of the forward model is to apply noise. We assign photometric uncertainties,  $\sigma'_X$ , by sampling an estimate of the true  $p(\sigma_X|f_X)$  of NSA galaxies. Then, we apply Gaussian noise

$$\hat{f}_X(\theta', z', \sigma'_x) = f_X(\theta', z') + n_X \quad \text{where } n_X \sim \mathcal{N}(0, \sigma'_X) \quad (4)$$

to derive the forward modeled photometric flux.

For our estimate of  $p(\sigma_X|f_X)$ , we use an empirical estimate of  $p(\sigma_X|f_X)$  based on NSA photometry and measured uncertainties. For each band, we separately estimate

$$\hat{p}(\sigma_X|f_X) = \mathcal{N}(\mu_{\sigma_X}(f_X), \sigma_{\sigma_X}(f_X)) \quad (5)$$

as a Gaussian in magnitude-space.  $\mu_{\sigma_X}$  and  $\sigma_{\sigma_X}$  are the median and standard deviation of  $\sigma_X$  as a function of  $f_X$  that we estimate by evaluating them in  $f_X$  bin and interpolating over the bins. Any  $\theta'$  that is assigned a negative  $\sigma'_X$  is removed from our training data. We also remove any training data with  $f_X(\theta')$  outside the range of NSA photometry. Although this is a simplistic noise model, we emphasize that our choice of noise model does not strongly affect the accuracy of the posteriors from SEDFLOW. This is because we design SEDFLOW to include  $\sigma_X$  in the conditional statement of the posterior. Hence, our primary concern is that  $\sigma'_X$  spans the observed  $\sigma_X$  values. We discuss this further in Section 5.1.

In total, we construct  $N_{\text{train}} = 1, 131, 561$  sets of SED parameters, redshift, photometric uncertainty, and mock NSA photometry:  $\{(\theta', z, \sigma'_X, \hat{f}_X)\}$ . There are 12 SED parameters and photometry and uncertainties in 5 NSA bands. In Figure 1, we present the training data through the joint distribution of a subset of  $\{(\theta', z, \sigma'_X, \hat{f}_X)\}$  (black). We include select SED model parameters ( $\log M_*$ ,  $\beta_1$ ), redshift, photometry ( $g$  and  $r$  bands), and photometric uncertainty ( $r$  band). We also include the distribution of redshift, photometry, and uncertainty of NSA galaxies (blue). The photometry and uncertainties are in magnitude-space. The distribution of the training data fully spans the distribution of NSA galaxies. Hence, the training data provides support over the full  $(f_X, \sigma_X, z)$  space of the NSA observations.

### 4.3. Training SEDFLOW

For SEDFLOW, we use a MAF normalizing flow model (Section 2.1) with 15 MADE blocks, each with 2 hidden layers and 500 hidden units. In total, the model has X free hyperparameters,  $\mathbf{h}$ . We determine this architecture through random hyperparameter search. Our goal is to determine  $\mathbf{h}$  of the MAF model,  $q(\theta|\mathbf{x}, \mathbf{h})$ , so that it accurately estimates the posterior probability distribution  $p(\theta|\mathbf{x})$ .  $\theta$  represent the SED parameters and  $\mathbf{x} = (f_X, \sigma_X, z)$ . We do this by minimizing the KL divergence between  $q(\theta|\mathbf{x}, \mathbf{h})$  and  $p(\theta|\mathbf{x})$ :  $D_{\text{KL}}(p||q)$ .

In practice, we split the training data (Section 4.2) into a training and validation set with a 90/10 split. Afterwards, we maximize the total log likelihood  $\sum_i \log q(\theta_i|\mathbf{x}_i, \mathbf{h})$  over training set, which is equivalent to minimizing  $D_{\text{KL}}(p||q)$ . We use the ADAM optimizer (Kingma & Ba 2017) with a learning rate of  $5 \times 10^{-4}$ . To prevent overfitting, we evaluate the total log likelihood on the validation data at every training epoch and stop the training when the validation log likelihood fails to increase after 20 epochs. Training our model with a batch size of 50 takes roughly a day on a single 2.6 GHz Intel Skylake CPU. Given our small batch size, we find similar training times when using CPUs or GPUs.

## 5. RESULTS

Now that we have trained our ANPE, we validate whether the posteriors we infer using it are accurate. As a first test, we compare the posterior from ANPE to the posterior derived from MCMC

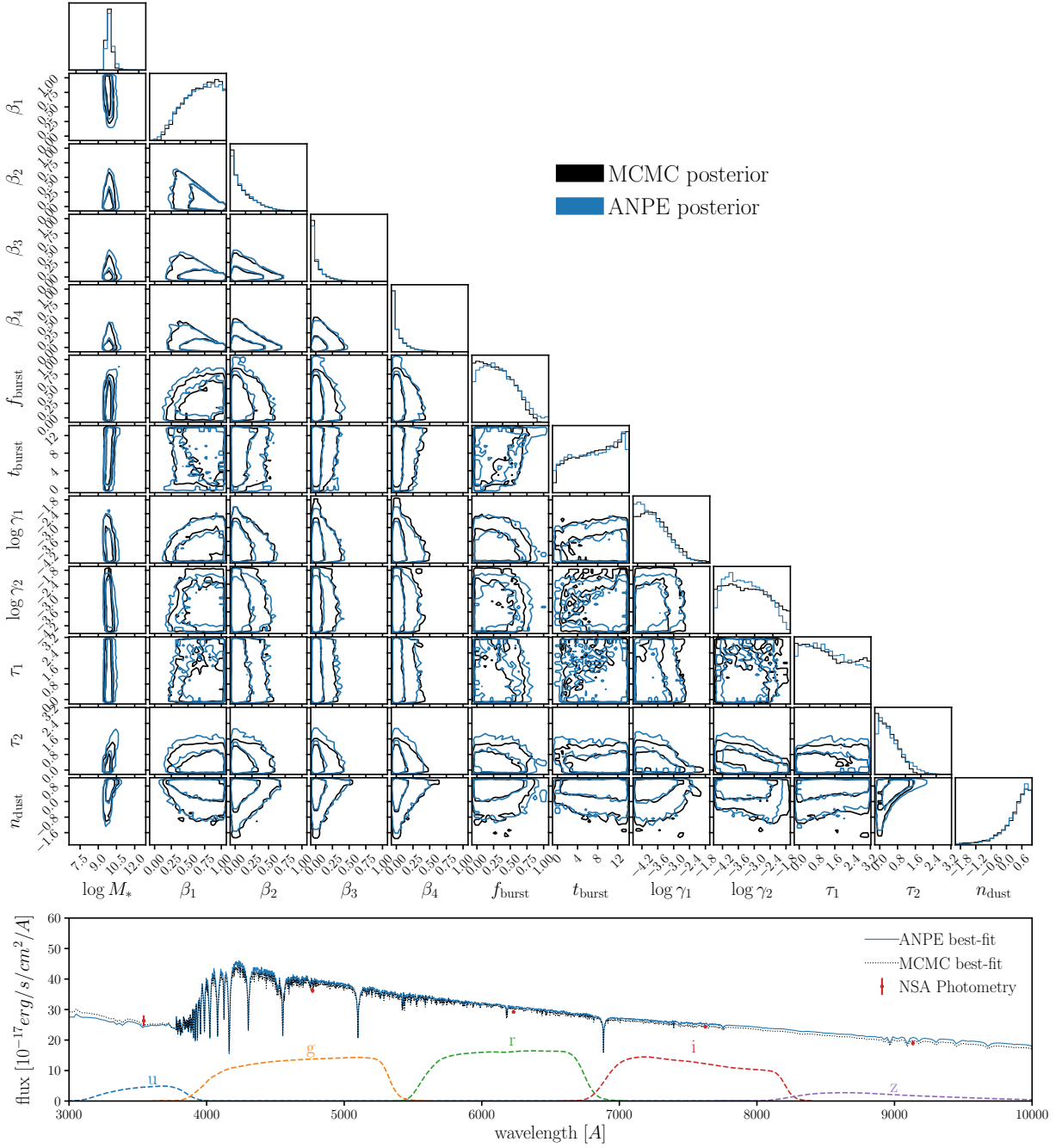


**Figure 2.** A comparison of the posteriors of the 12 SED model parameters derived from standard MCMC sampling (black) and our ANPE (blue) for a single arbitrarily selected NSA galaxy. The posteriors are in excellent agreement for all of the parameters. Estimating the posterior using MCMC sampling requires X hours. Even using neural emulators to accelerate likelihood evaluations, MCMC sampling requires Y hours. *With ANPE, inferring the full posterior requires 1 second per galaxy.*

sampling for a single arbitrarily chosen NSA galaxy in Figure 2. In the top, we present the the posterior distribution of the 12 SED model parameters (Section 4.1) for the ANPE posterior (blue) and MCMC posterior (black). *The ANPE posterior is in excellent agreement with the MCMC posterior for all of the SED parameters.*

In the bottom of Figure 2, we compare the SED distributions of the best-fit parameter values from the ANPE (blue) and MCMC posteriors (black dotted). We also include the NSA photometric flux of the selected galaxy (red) and mark the optical broadband response curves (dashed). The best-fit SED from the ANPE posterior is also in good agreement with both the MCMC best-fit and the NSA photometry.

The key advantage of ANPE is that it enables accurate Bayesian inference orders of magnitude faster than conventional methods. We derive the MCMC posterior using the ZEUS ensemble slice-sampler (Karamanis & Beutler 2020) with 30 walkers and 10,000 iterations. 2,000 of the iterations are discarded for burn-in. In total, the MCMC posterior requires  $>100,000$  SED model evaluations. Since each evaluation takes  $\sim 340$  ms, it  $\sim 10$  CPU hours for a single MCMC posterior. SED modeling has recently adopted neural emulators to accelerate SED model evaluations. In Hahn et al. (2022), for instance, the PROVABGS emulator takes  $\sim 2.9$  ms to evaluate,  $> 100\times$  faster than the original model. Yet, even with emulators, due to the number of evaluations necessary for convergence, an MCMC posterior takes  $\sim 10$  CPU minutes. Meanwhile, after training, *the ANPE posterior takes 1 second —  $>10^5\times$  faster than MCMC.*

Besides the selected NSA galaxy in Figure 2, the posteriors from ANPE and MCMC are overall in excellent for NSA galaxies. However, we do not know the true SED parameters for these galaxies so to further validate the ANPE posteriors, we use test synthetic photometry, where we know the truth. We sample 1000 SED parameters from the prior,  $\{\theta_i^{\text{test}}\} \sim p(\theta)$ , and construct synthetic NSA galaxy photometry,  $\{\mathbf{x}_i^{\text{test}}\}$ , for them in the same way as the training data in Section 4.2. Afterwards, we generate posteriors for each of test data using our ANPE:  $\{p(\theta | \mathbf{x}_i^{\text{test}})\}$ .

In Figure 3, we present the probability-probability (p-p) plot of the ANPE posteriors for the test data. The p-p plot presents the cumulative distribution function (CDF) of the percentile score of the true value within the marginalized posterior for each SED parameter. For the true posterior, the percentiles are uniformly distributed so the CDF is a diagonal (black dashed). *Overall, the ANPE posteriors are in good agreement with the true posteriors for each of the SED parameters.*

We also include in Figure 3 the CDFs of the SED parameters for the MCMC posteriors derived for a subset of 100 test galaxy photometry (gray dotted). Based on the CDFs, the ANPE posteriors are actually in better agreement with the true posteriors than those derived from MCMC. This is due to the fact that MCMC posteriors are only estimates of the true posterior and are subject to limitations in initialization, sampling, and convergence. Meanwhile, these limitations do not impact posteriors from ANPE and so the comparison highlights additional advantages of ANPE besides the  $10^5\times$  speed up.

We examine another validation of the ANPE posteriors using simulation-based calibration (SBC; Talts et al. 2020). Rather than using percentile scores, SBC examines the distribution of the rank statistics of the true parameter values within the marginalized posteriors. It addresses the fact that the

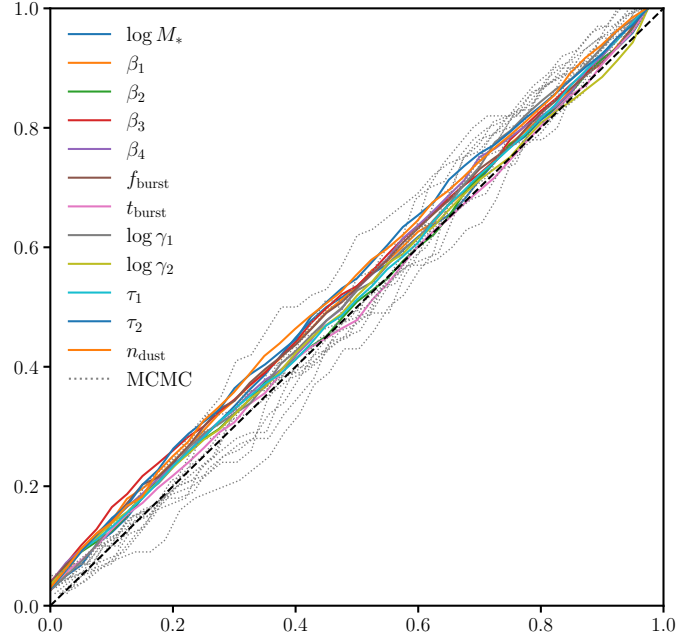


**Figure 3.** Probability-probability (p-p) plot of the ANPE for 1000 simulated test data. For each SED parameter, we plot the cumulative distribution function (CDF) of the percentile score of the true value within the ANPE marginalized posterior. For the true posteriors, the percentile score is uniformly distributed so the CDF is diagonal (black dashed). The test data is constructed in the same way as the training data (Section 4.2). For reference, we include the p-p plot of the posterior estimated from MCMC sampling (gray). *The ANPE is in good agreement the true posterior.*

CDFs only asymptotically approach the true values and that the discrete sampling of the posterior can cause artifacts in the CDFs. In Figure 4, we present SBC of each SED model parameter for the ANPE posteriors (blue) using the 1000 test data. For comparison, we include the SBC for the MCMC posteriors (gray dotted). Similar to the percentile score, the distribution of the rank statistic is uniform for the true posterior (black dashed). The distribution of rank statistic for the ANPE posteriors are overall in good agreement with a uniform distribution. Hence, the ANPE posteriors are in good agreement with the true posterior.

An advantage of SBC is that by examining the deviation of rank statistics distribution from uniformity, we can determine how the ANPE posteriors deviate from the true posteriors. For most of the SED parameters, we find little deviation from uniformity so the ANPE posterior is accurate. However, we find a noticeable deviation for  $\log \gamma_2$ , the coefficient of the second ZH NMF basis function. The rank statistic distribution of  $\log \gamma_2$  has a symmetric U shape where the true parameter values are more often at the lowest and highest ranks. This means that on average the ANPE posterior for  $\log \gamma_2$  is narrower than the true posterior and underestimates the uncertainty. To better gauge the actual impact of such a discrepancy, we examine the distributions of the MCMC posterior. Since we only use 100 test data for MCMC the distributions are noisy; however, we find overall significantly large discrepancies from uniformity (see *e.g.*  $\log M_*$  and  $\beta_4$  panels). Based on this comparison, we



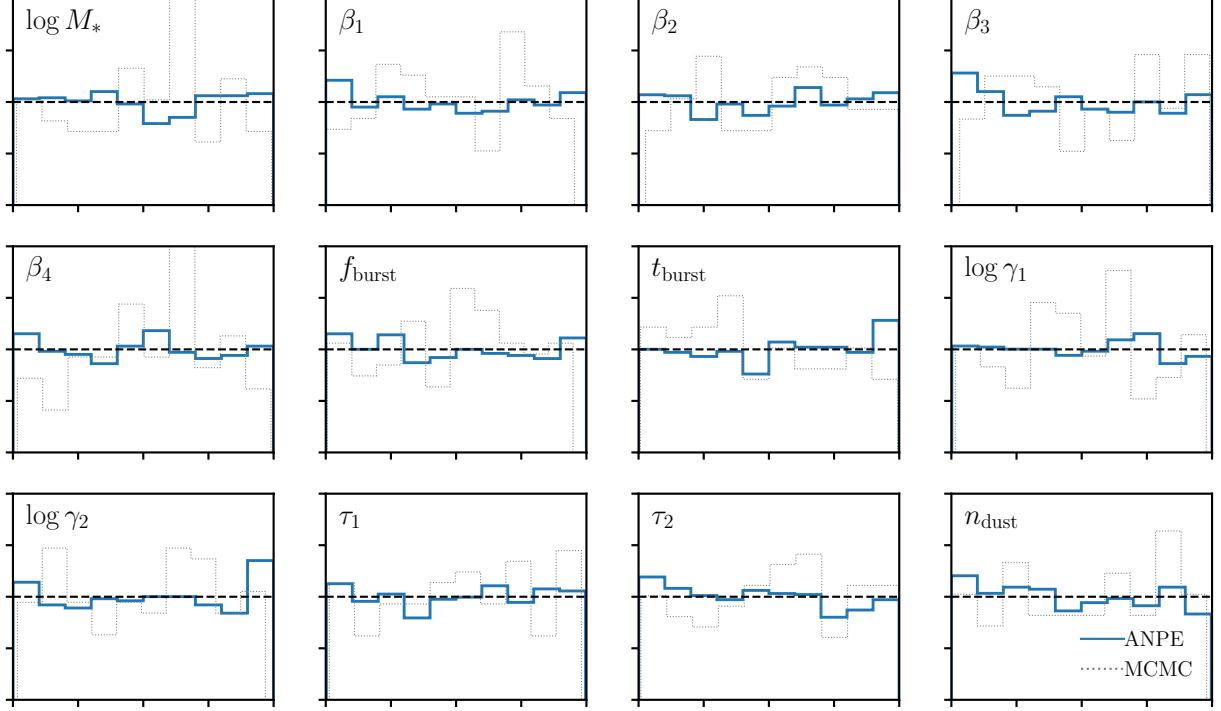


**Figure 4.** Simulation-based calibration plot of the ANPE for 1000 simulated test data. For each SED parameter, we plot the histogram of the rank statistic of the true value within the marginalized ANPE posterior (blue). For the true posterior, the rank statistics will have a uniform distribution (black dashed). For reference, we include the rank distribution of the MCMC posterior for a subset of 100 test data (gray dotted). *The ANPE is in good agreement the true posterior.*

conclude that our ANPE produces posteriors that are in good agreement with the true posteriors. *revisit once we have the final ANPE*

With the accuracy of our ANPE validated, we now apply it to derive posteriors for all of our NSA galaxies (Section 3). *elaborate on this* We make the

TODO

### 5.1. Discussion

With ANPE, we can generate posteriors for SED modeling  $>10^5$  faster than conventional MCMC-based methods. The primary concern for ANPE is the accuracy of the posteriors. One of the key factors that determines the accuracy of the ANPE is the training data. To construct our training data, we use a simple noise model with a Gaussian estimate of  $p(\sigma_X | f_X)$  and treat each photometric band separately, ignoring any covariance (Section 4.2). The actual  $p(\sigma_X | f_x)$  distribution for NSA, as Figure 1 illustrates, is not Gaussian. There are also significant covariances among the photometry in different bands. Despite the shortcomings of our training data, our ANPE is *not* sensitive to the accuracy of our noise model. This is because we include  $\sigma_X$  as a conditional variable in our ANPE (Section 4.3). Hence, as long as the observed  $\mathbf{x}_{\text{obs}} = (f_X, \sigma_X, z)$  is sufficiently within the  $\mathbf{x}$ -space support of the training data, the ANPE produces accurate posteriors.

A more accurate noise model would in principle improve the performance of ANPEs since the  $\mathbf{x}$ -space of the training data will more effectively span the observations. In other words, there will be fewer training data expended in regions of  $\mathbf{x}$ -space that are not occupied by observations. However, for our application to SED modeling, we do not find significantly better performance when we replace the noise model to a more sophisticated one. Instead, we find that having a sufficient number of training data is a more important factor for the accuracy of the ANPE. For instance, we find significantly lower accuracy in the posteriors when we use less than  $<500,000$  training data points.

The ANPE produces accurate posteriors for  $\mathbf{x}_{\text{obs}}$  within the  $\mathbf{x}$  support of the training data. However, some objects in the NSA catalog are outside of the support. For instance, the  $g$ ,  $r$ ,  $\sigma_r$  panels of Figure 1 reveal a number of NSA objects (blue) that lie outside of the  $g - r$  color distribution of the training data (black). This is not due to deficiencies in the noise model since the  $g - \sigma_r$  and  $r - \sigma_r$  relations of these NSA objects are within that of the training data. Some of these objects are likely observational artifacts. Even with the quality cuts in Section 3, there are likely objects in our samples with problematic photometry. [list a few typical examples of problematic photometry](#). The SEDs of such artifacts cannot be modeled using an SPS model combined with noise, so they can lie outside of the training  $\mathbf{x}$  support.

Alternatively, the training data may provide insufficient support because the SED model we use to generate them does not sufficiently describe the full range of true galaxy SEDs. In this work we use the PROVABGS SED model (Section 4.1 and ?). This model provides compact and flexible prescriptions for SFH and ZH that can describe a broad range of SFHs and ZHs (?). However, the prescriptions were derived from the SFHs and ZHs of simulated galaxies in Illustris, which may not reflect the full range of SFHs and ZHs of actual galaxies. Even if the PROVABGS SFH and ZH prescriptions can accurately describe the true SFH and ZH, there are limitations in our understanding of stellar evolution.

There is currently no firm consensus in SPS: *e.g.* stellar evolution, stellar spectral libraries, or the IMF (*e.g.* ?????). The PROVABGS model uses MIST isochrones, [Chabrier \(2003\)](#) IMF, and the MILES + BaSeL spectral libraries. These choices limit the range of SED that can be produced by the training data. For instance, if galaxies have significant variations in their IMF, assuming a fixed IMF would reduce the  $\mathbf{x}$  support of our training data. A more flexible SED model that includes uncertainties in SPS would widen the range of galaxy SEDs that can be modeled. Data-driven approaches may also enable SED models to be more descriptive (*e.g.* [Hogg et al. 2016](#); [Portillo et al. 2020](#)). Extending SED models, however, is beyond the scope of this work, which focuses on improving the Bayesian framework for SED modeling. We emphasize that conventional approaches with MCMC are *equally* impacted by the limitations of the SED model.

In Section 5, we assessed the accuracy of the ANPE posteriors using posteriors derived using MCMC and test SEDs, where we know the true parameter values. Both cases demonstrate the sufficient accuracy of ANPE posteriors for this work. However, for applications that require even higher fidelity posteriors, there are further tests. For instance, the  $\chi^2$  of the best-fit parameter value from the ANPE posterior can be used to test whether the best-fit SED model accurately reproduces the observed SED. This only requires one additional SED model evaluation per galaxy.

For an even more rigorous test of the posteriors, one can construct an Amortized Neural Likelihood Estimator (ANLE) using the same training data and neural density estimator setup. Unlike the ANPE, which estimates  $p(\theta | f_X, \sigma_X, z)$ , the ANLE estimates  $p(f_X | \theta, \sigma_X, z)$ . We can then further validate the posteriors by assessing whether the observed photometry lies within the ANLE.

In this work, the ANPE estimates a 12-dimensional probability distribution with an 11-dimensional conditional variable space. However, future SED modeling will likely require higher dimensionality. As mention above, SED models currently do not account for uncertainties in stellar evolution, spectral libraries, or the IMF. Including these uncertainties as well as any additional parameters to account for observational systematics (*e.g.* zero-point calibration, see also <http://www.nsatlas.org/caveats>) will significantly increase the dimensionality of the posterior. Higher dimensionality significantly increases the computational cost of current methods: the number of evaluation scales roughly linearly with the number of dimensions for MCMC. Fortunately, ANPE has already been applied to higher dimensional applications. Dax et al. (2021), for instance, constructed an accurate ANPE for a 15-dimensional model parameter space and 128-dimensional conditional variable space.

We demonstrate that we can exploit ANPE to accelerate SED modeling of galaxy photometry. The next step is to apply ANPE to SED modeling of galaxy spectra. Constructing an ANPE for the full data space of spectra, however, requires estimating a dramatically higher dimensional probability distribution. SDSS spectra, for instance, have **X** spectral elements. Furthermore, in our approach we include the uncertainties as conditional variables and double the curse of dimensionality. Recent works, however, have demonstrated that galaxy spectra can be represented in a compact low-dimensional space using autoencoders (Portillo et al. 2020, ; Melchior & Hahn in prep.). In Portillo et al. (2020), they demonstrate that SDSS galaxy spectra can be compressed into 10-dimensional latent variable space with little loss of information. With this spectral compression, we can dramatically reduce the dimensionality of the conditional variable space. We will explore SED modeling of galaxy spectrophotometry using ANPE and spectral compression in a following work.

One of the key ingredients in Bayesian inference is the prior. For SED modeling, recent works have demonstrated that model priors play a crucial role in the derived galaxy properties (Carnall et al. 2018; Leja et al. 2019a; ?). Even “uninformative” uniform priors on SED model parameters can impose undesirable priors on derived galaxy properties such as  $M_*$ , SFR, SFH, or ZH. This underscores the importance of carefully selecting priors and validating results using multiple different priors. For SED modeling with MCMC, selecting a different prior requires reevaluating posteriors for every galaxy. This means repeating all the SED model evaluations in the MCMC sampling. For ANPE, the prior is set by how the parameters of the training data are sampled. For a new prior, we can subsample the training data so that its parameters follow a newly selected prior. Afterwards, the ANPE can be re-trained, re-validated on the test data, and re-deployed on the entire dataset. Re-training the ANPE has significant computational cost, however, it requires no where near the Hence, ANPE has the additional advantage that we can vary the prior without additional model evaluations.

**extra advantages of faster posteriors** reemphasize that we can meet the needs of DESI, PFS, Rubin, JWST, and Roman.

TODO

TODO

## 6. SUMMARY

By analyzing the SED of a galaxy, we can infer detailed physical properties such as its stellar mass, star formation rate, metallicity, and dust content. These properties serve as the building blocks of our understanding of how galaxies form and evolve. State-of-the-art SED modeling methods use MCMC sampling to perform Bayesian statistical inference. They derive posterior probability distributions of galaxy properties given observation that accurately estimate uncertainties and parameter degeneracies. Posteriors also enable marginalization over any nuisance parameters. For the dimensionality of current SED models, deriving a posterior requires  $\gtrsim 100,000$  model evaluations and take  $\gtrsim 10 - 100$  CPU hours per galaxy. Upcoming galaxy surveys, however, will observe *millions* of galaxies using *e.g.* DESI, PFS, Rubin observatory, James Webb Space Telescope, and the Roman Space Telescope. Analyzing all of these galaxies with current Bayesian SED models is infeasible and would require *billions* of CPU hours. Rigorous inference will soon be the major bottleneck for galaxy studies.

We demonstrate in this work that Amortized Neural Posterior Estimation (ANPE) provides an alternative *scalable* approach for Bayesian inference in SED modeling. ANPE is a simulation-based inference method that leverages the latest developments in ML. It formulates Bayesian inference into a density estimation problem and uses neural density estimators (NDE) to estimate the posterior over the full space of observations. The NDE is trained using parameter values drawn from the prior and mock observations constructed using them and a forward model. Once trained, a posterior can be derived using the NDE by plugging in the observations as the conditional variables without any additional model evaluations.

In this work, we present SEDFLOW, a galaxy SED modeling method using ANPE and PROVABGS, a flexible SED model that uses a compact non-parametric SFH and ZH prescriptions and was recently validated in ?. Furthermore, we apply SEDFLOW to optical photometry from the NASA-Sloan Atlas as demonstration and validation of our ANPE approach. In our analysis we present the key results below.

- We train SEDFLOW using a data set of  $\sim 1$  million SED model parameters and synthetic SEDs constructed using them and a forward model. The parameters are drawn from a prior and the forward model is based on PROVABGS and a Gaussian photometric noise model. We design the ANPE to estimate  $p(\theta|f_X, \sigma_X, z)$ , where  $f_X$ ,  $\sigma_X$ , and  $z$  are the photometry, photometric uncertainty, and redshift respectively. For its architecture, we use a MAF normalizing flow with 15 MADE blocks each with 2 hidden layers and 500 hidden units. Training SEDFLOW requires roughly 1 day on a single CPU. Once trained, deriving posteriors of galaxy properties for a galaxy takes  $\sim 1$  second —  $5 \times 10^4 \times$  faster than current methods.
- Posteriors derived using SEDFLOW show excellent agreement with posteriors derived from MCMC sampling. We further validate the accuracy of its posteriors by applying SEDFLOW to synthetic observations with known true parameter values. Based on statistical metrics used in the literature (p-p plot and SBC), we find excellent agreement between the SEDFLOW and the true posterior.

- Lastly, we demonstrate the advantages of SEDFLOW by applying it to the NASA-Sloan Atlas. Estimating the posterior of  $\sim 34,000$  galaxies takes **X** CPU hours. We make the catalog of posteriors publicly available at [urlhere](#). For each galaxy, the catalog contains posteriors on all 12 PROVABGS SED model parameters. In terms of galaxy properties, the catalog includes posteriors of  $M_*$ , average SFR over 1Gyr, mass-weighted metallicity, mass-weighted age, and dust optical depth.

TODO

Our work clearly highlights the advantages of using an ANPE approach to SED modeling. Such scalable methods for Bayesian SED modeling will enable us to analyze the millions of galaxies that will be observed by upcoming experiments. As we discuss in Section 5.1, however, an ANPE approach requires careful construction of the training data. Its accuracy depends on quality of the forward model and limitations in, say, the SED model can impact the accuracy of the ANPE posteriors outside of the training data support. These are equally important considerations and limitations in current SED modeling methods. In this work, we focus on SED modeling of optical photometry; however, SEDFLOW can easily be extended to multi-wavelength photometry. In fact, with the latest developments in efficiently dimensionality reduction of spectra (Portillo et al. 2020, , Melchior & Hahn 2022), SEDFLOW can even be extended to galaxy spectra. We will explore this in subsequent work.

## ACKNOWLEDGEMENTS

It's a pleasure to thank Adam Carnall, Miles Cranmer, Kartheik Iyer, Andy Goulding, Jenny E. Green, Uroš Seljak, Michael A. Strauss, ... for valuable discussions and comments.

## APPENDIX

## REFERENCES

- Acquaviva, V., Gawiser, E., & Guaita, L. 2011, *The Astrophysical Journal*, 737, 47, doi: [10.1088/0004-637X/737/2/47](#)
- Ahumada, R., Prieto, C. A., Almeida, A., et al. 2020, *The Astrophysical Journal Supplement Series*, 249, 3, doi: [10.3847/1538-4365/ab929e](#)
- Aihara, H., Allende Prieto, C., An, D., et al. 2011, *The Astrophysical Journal Supplement Series*, 193, 29, doi: [10.1088/0067-0049/193/2/29](#)
- Alsing, J., Charnock, T., Feeney, S., & Wandelt, B. 2019, *Monthly Notices of the Royal Astronomical Society*, 488, 4440, doi: [10.1093/mnras/stz1960](#)
- Alsing, J., Wandelt, B., & Feeney, S. 2018, *arXiv:1801.01497 [astro-ph]*, <https://arxiv.org/abs/1801.01497>
- Baldry, I. K., Liske, J., Brown, M. J. I., et al. 2018, *Monthly Notices of the Royal Astronomical Society*, 474, 3875, doi: [10.1093/mnras/stx3042](#)
- Beaumont, M. A., Zhang, W., & Balding, D. J. 2002, *Genetics*, 162, 2025
- Blanton, M. R., Kazin, E., Muna, D., Weaver, B. A., & Price-Whelan, A. 2011, *The Astronomical Journal*, 142, 31, doi: [10.1088/0004-6256/142/1/31](#)
- Brehmer, J., Louppe, G., Pavez, J., & Cranmer, K. 2019, *arXiv:1805.12244 [hep-ph, physics:physics, stat]*, <https://arxiv.org/abs/1805.12244>
- Bruzual, G., & Charlot, S. 2003, *Monthly Notices of the Royal Astronomical Society*, 344, 1000, doi: [10.1046/j.1365-8711.2003.06897.x](#)



- Burgarella, D., Buat, V., & Iglesias-Páramo, J. 2005, *Monthly Notices of the Royal Astronomical Society*, 360, 1413, doi: [10.1111/j.1365-2966.2005.09131.x](https://doi.org/10.1111/j.1365-2966.2005.09131.x)
- Cameron, E., & Pettitt, A. N. 2012, *Monthly Notices of the Royal Astronomical Society*, 425, 44, doi: [10.1111/j.1365-2966.2012.21371.x](https://doi.org/10.1111/j.1365-2966.2012.21371.x)
- Carnall, A. C., Leja, J., Johnson, B. D., et al. 2018, arXiv:1811.03635 [astro-ph]. <https://arxiv.org/abs/1811.03635>
- Carnall, A. C., McLure, R. J., Dunlop, J. S., & Davé, R. 2017, arXiv:1712.04452 [astro-ph]. <https://arxiv.org/abs/1712.04452>
- Chabrier, G. 2003, *Publications of the Astronomical Society of the Pacific*, 115, 763, doi: [10.1086/376392](https://doi.org/10.1086/376392)
- Charlot, S., & Fall, S. M. 2000, *The Astrophysical Journal*, 539, 718, doi: [10.1086/309250](https://doi.org/10.1086/309250)
- Chevallard, J., & Charlot, S. 2016, *Monthly Notices of the Royal Astronomical Society*, 462, 1415, doi: [10.1093/mnras/stw1756](https://doi.org/10.1093/mnras/stw1756)
- Choi, J., Dotter, A., Conroy, C., et al. 2016, *The Astrophysical Journal*, 823, 102, doi: [10.3847/0004-637X/823/2/102](https://doi.org/10.3847/0004-637X/823/2/102)
- Cichocki, A., & Phan, A.-H. 2009, *IEICE Transactions on Fundamentals of Electronics Communications and Computer Sciences*, 92, 708, doi: [10.1587/transfun.E92.A.708](https://doi.org/10.1587/transfun.E92.A.708)
- Cid Fernandes, R., Mateus, A., Sodré, L., Stasińska, G., & Gomes, J. M. 2005, *Monthly Notices of the Royal Astronomical Society*, 358, 363, doi: [10.1111/j.1365-2966.2005.08752.x](https://doi.org/10.1111/j.1365-2966.2005.08752.x)
- Collaboration, D., Aghamousa, A., Aguilar, J., et al. 2016, arXiv:1611.00036 [astro-ph]. <https://arxiv.org/abs/1611.00036>
- Conroy, C. 2013, *Annual Review of Astronomy and Astrophysics*, 51, 393, doi: [10.1146/annurev-astro-082812-141017](https://doi.org/10.1146/annurev-astro-082812-141017)
- Conroy, C., & Gunn, J. E. 2010, *The Astrophysical Journal*, 712, 833, doi: [10.1088/0004-637X/712/2/833](https://doi.org/10.1088/0004-637X/712/2/833)
- Conroy, C., Gunn, J. E., & White, M. 2009, *The Astrophysical Journal*, 699, 486, doi: [10.1088/0004-637X/699/1/486](https://doi.org/10.1088/0004-637X/699/1/486)
- Cranmer, K., Brehmer, J., & Louppe, G. 2020, *Proceedings of the National Academy of Sciences*, 117, 30055, doi: [10.1073/pnas.1912789117](https://doi.org/10.1073/pnas.1912789117)
- da Cunha, E., Charlot, S., & Elbaz, D. 2008, *Monthly Notices of the Royal Astronomical Society*, 388, 1595, doi: [10.1111/j.1365-2966.2008.13535.x](https://doi.org/10.1111/j.1365-2966.2008.13535.x)
- Davis, M., Faber, S. M., Newman, J., et al. 2003, 4834, 161, doi: [10.1117/12.457897](https://doi.org/10.1117/12.457897)
- Dax, M., Green, S. R., Gair, J., et al. 2021, arXiv:2106.12594 [astro-ph, physics:gr-qc]. <https://arxiv.org/abs/2106.12594>
- Dotter, A. 2016, *The Astrophysical Journal Supplement Series*, 222, 8, doi: [10.3847/0067-0049/222/1/8](https://doi.org/10.3847/0067-0049/222/1/8)
- Durkan, C., Bekasov, A., Murray, I., & Papamakarios, G. 2019, arXiv:1906.04032 [cs, stat]. <https://arxiv.org/abs/1906.04032>
- Févotte, C., & Idier, J. 2011, arXiv:1010.1763 [cs]. <https://arxiv.org/abs/1010.1763>
- Genel, S., Vogelsberger, M., Springel, V., et al. 2014, *Monthly Notices of the Royal Astronomical Society*, 445, 175, doi: [10.1093/mnras/stu1654](https://doi.org/10.1093/mnras/stu1654)
- Germain, M., Gregor, K., Murray, I., & Larochelle, H. 2015, arXiv:1502.03509 [cs, stat]. <https://arxiv.org/abs/1502.03509>
- Greenberg, D. S., Nonnenmacher, M., & Macke, J. H. 2019, *Automatic Posterior Transformation for Likelihood-Free Inference*
- Hahn, C., Beutler, F., Sinha, M., et al. 2019, *Monthly Notices of the Royal Astronomical Society*, 485, 2956, doi: [10.1093/mnras/stz558](https://doi.org/10.1093/mnras/stz558)
- Hahn, C., Vakili, M., Walsh, K., et al. 2017, *Monthly Notices of the Royal Astronomical Society*, 469, 2791, doi: [10.1093/mnras/stx894](https://doi.org/10.1093/mnras/stx894)
- Hogg, D. W., Casey, A. R., Ness, M., et al. 2016, arXiv:1601.05413 [astro-ph], doi: [10.3847/1538-4357/833/2/262](https://doi.org/10.3847/1538-4357/833/2/262)
- Huppenkothen, D., & Bachetti, M. 2021, *Accurate X-ray Timing in the Presence of Systematic Biases With Simulation-Based Inference*
- Ivezić, Ž., Kahn, S. M., Tyson, J. A., et al. 2019, *The Astrophysical Journal*, 873, 111, doi: [10.3847/1538-4357/ab042c](https://doi.org/10.3847/1538-4357/ab042c)
- Johnson, B. D., Leja, J., Conroy, C., & Speagle, J. S. 2021, *The Astrophysical Journal Supplement Series*, 254, 22, doi: [10.3847/1538-4365/abef67](https://doi.org/10.3847/1538-4365/abef67)
- Kacprzak, T., Herbel, J., Amara, A., & Réfrégier, A. 2018, *Journal of Cosmology and Astro-Particle Physics*, 2018, 042, doi: [10.1088/1475-7516/2018/02/042](https://doi.org/10.1088/1475-7516/2018/02/042)

- Karamanis, M., & Beutler, F. 2020, arXiv e-prints, arXiv:2002.06212
- Kauffmann, G., Heckman, T. M., White, S. D. M., et al. 2003, *Monthly Notices of the Royal Astronomical Society*, 341, 33, doi: [10.1046/j.1365-8711.2003.06291.x](https://doi.org/10.1046/j.1365-8711.2003.06291.x)
- Kingma, D. P., & Ba, J. 2017, arXiv:1412.6980 [cs]. <https://arxiv.org/abs/1412.6980>
- Koleva, M., Prugniel, P., Ocvirk, P., Le Borgne, D., & Soubiran, C. 2008, *Monthly Notices of the Royal Astronomical Society*, 385, 1998, doi: [10.1111/j.1365-2966.2008.12908.x](https://doi.org/10.1111/j.1365-2966.2008.12908.x)
- Kriek, M., & Conroy, C. 2013, *The Astrophysical Journal Letters*, 775, L16, doi: [10.1088/2041-8205/775/1/L16](https://doi.org/10.1088/2041-8205/775/1/L16)
- Lee, D. D., & Seung, H. S. 1999, *Nature*, 401, 788, doi: [10.1038/44565](https://doi.org/10.1038/44565)
- Leja, J., Carnall, A. C., Johnson, B. D., Conroy, C., & Speagle, J. S. 2019a, *ApJ*, 876, 3, doi: [10.3847/1538-4357/ab133c](https://doi.org/10.3847/1538-4357/ab133c)
- Leja, J., Johnson, B. D., Conroy, C., van Dokkum, P. G., & Byler, N. 2017, *The Astrophysical Journal*, 837, 170, doi: [10.3847/1538-4357/aa5ffe](https://doi.org/10.3847/1538-4357/aa5ffe)
- Leja, J., Speagle, J. S., Johnson, B. D., et al. 2019b, arXiv, arXiv:1910.04168
- Lejeune, T., Cuisinier, F., & Buser, R. 1997, *A & A Supplement series*, Vol. 125, October II 1997, p.229-246., 125, 229, doi: [10.1051/aas:1997373](https://doi.org/10.1051/aas:1997373)
- . 1998, *Astronomy and Astrophysics Supplement*, v.130, p.65-75, 130, 65, doi: [10.1051/aas:1998405](https://doi.org/10.1051/aas:1998405)
- Lilly, S. J., Le Fèvre, O., Renzini, A., et al. 2007, *The Astrophysical Journal Supplement Series*, 172, 70, doi: [10.1086/516589](https://doi.org/10.1086/516589)
- Maraston, C. 2005, *Monthly Notices of the Royal Astronomical Society*, 362, 799, doi: [10.1111/j.1365-2966.2005.09270.x](https://doi.org/10.1111/j.1365-2966.2005.09270.x)
- Nelson, D., Pillepich, A., Genel, S., et al. 2015, *Astronomy and Computing*, 13, 12, doi: [10.1016/j.ascom.2015.09.003](https://doi.org/10.1016/j.ascom.2015.09.003)
- Papamakarios, G., Pavlakou, T., & Murray, I. 2017, arXiv e-prints, 1705, arXiv:1705.07057
- Paxton, B., Bildsten, L., Dotter, A., et al. 2011, *The Astrophysical Journal Supplement Series*, 192, 3, doi: [10.1088/0067-0049/192/1/3](https://doi.org/10.1088/0067-0049/192/1/3)
- Paxton, B., Cantiello, M., Arras, P., et al. 2013, *The Astrophysical Journal Supplement Series*, 208, 4, doi: [10.1088/0067-0049/208/1/4](https://doi.org/10.1088/0067-0049/208/1/4)
- Paxton, B., Marchant, P., Schwab, J., et al. 2015, *The Astrophysical Journal Supplement Series*, 220, 15, doi: [10.1088/0067-0049/220/1/15](https://doi.org/10.1088/0067-0049/220/1/15)
- Portillo, S. K. N., Parejko, J. K., Vergara, J. R., & Connolly, A. J. 2020, *The Astronomical Journal*, 160, 45, doi: [10.3847/1538-3881/ab9644](https://doi.org/10.3847/1538-3881/ab9644)
- Pritchard, J. K., Seielstad, M. T., Perez-Lezaun, A., & Feldman, M. W. 1999, *Molecular Biology and Evolution*, 16, 1791, doi: [10.1093/oxfordjournals.molbev.a026091](https://doi.org/10.1093/oxfordjournals.molbev.a026091)
- Rubin, D. B. 1984, *The Annals of Statistics*, 12, 1151
- Ruiz-Macias, O., Zarrouk, P., Cole, S., et al. 2021, *Monthly Notices of the Royal Astronomical Society*, 502, 4328, doi: [10.1093/mnras/stab292](https://doi.org/10.1093/mnras/stab292)
- Salim, S., Rich, R. M., Charlot, S., et al. 2007, *The Astrophysical Journal Supplement Series*, 173, 267, doi: [10.1086/519218](https://doi.org/10.1086/519218)
- Sánchez-Blázquez, P., Peletier, R. F., Jiménez-Vicente, J., et al. 2006, *Monthly Notices of the Royal Astronomical Society*, 371, 703, doi: [10.1111/j.1365-2966.2006.10699.x](https://doi.org/10.1111/j.1365-2966.2006.10699.x)
- Schlegel, D. J., Finkbeiner, D. P., & Davis, M. 1998, *The Astrophysical Journal*, 500, 525, doi: [10.1086/305772](https://doi.org/10.1086/305772)
- Scoville, N., Aussel, H., Brusa, M., et al. 2007, *The Astrophysical Journal Supplement Series*, 172, 1, doi: [10.1086/516585](https://doi.org/10.1086/516585)
- Spergel, D., Gehrels, N., Baltay, C., et al. 2015, *Wide-Field Infrared Survey Telescope-Astrophysics Focused Telescope Assets WFIRST-AFTA 2015 Report*
- Stein, G., Seljak, U., & Dai, B. 2020, *Unsupervised In-Distribution Anomaly Detection of New Physics through Conditional Density Estimation*
- Tabak, E. G., & Turner, C. V. 2013, *Communications on Pure and Applied Mathematics*, 66, 145, doi: [10.1002/cpa.21423](https://doi.org/10.1002/cpa.21423)
- Tabak, E. G., & Vanden-Eijnden, E. 2010, *Communications in Mathematical Sciences*, 8, 217, doi: [10.4310/CMS.2010.v8.n1.a11](https://doi.org/10.4310/CMS.2010.v8.n1.a11)
- Tacchella, S., Conroy, C., Faber, S. M., et al. 2021, arXiv e-prints, 2102, arXiv:2102.12494
- Takada, M., Ellis, R. S., Chiba, M., et al. 2014, *Publications of the Astronomical Society of Japan*, 66, R1, doi: [10.1093/pasj/pst019](https://doi.org/10.1093/pasj/pst019)
- Talts, S., Betancourt, M., Simpson, D., Vehtari, A., & Gelman, A. 2020, arXiv:1804.06788 [stat]. <https://arxiv.org/abs/1804.06788>

- Tejero-Cantero, A., Boelts, J., Deistler, M., et al. 2020, *Journal of Open Source Software*, 5, 2505, doi: [10.21105/joss.02505](https://doi.org/10.21105/joss.02505)
- Thorne, J. E., Robotham, A. S. G., Davies, L. J. M., et al. 2021, *Monthly Notices of the Royal Astronomical Society*, 505, 540, doi: [10.1093/mnras/stab1294](https://doi.org/10.1093/mnras/stab1294)
- Tojeiro, R., Heavens, A. F., Jimenez, R., & Panter, B. 2007, *Monthly Notices of the Royal Astronomical Society*, 381, 1252, doi: [10.1111/j.1365-2966.2007.12323.x](https://doi.org/10.1111/j.1365-2966.2007.12323.x)
- Uria, B., Côté, M.-A., Gregor, K., Murray, I., & Larochelle, H. 2016, arXiv:1605.02226 [cs]. <https://arxiv.org/abs/1605.02226>
- Vogelsberger, M., Genel, S., Springel, V., et al. 2014, *Monthly Notices of the Royal Astronomical Society*, 444, 1518, doi: [10.1093/mnras/stu1536](https://doi.org/10.1093/mnras/stu1536)
- Walcher, J., Groves, B., Budavári, T., & Dale, D. 2011, *Astrophysics and Space Science*, 331, 1, doi: [10.1007/s10509-010-0458-z](https://doi.org/10.1007/s10509-010-0458-z)
- Westera, P., Lejeune, T., Buser, R., Cuisinier, F., & Bruzual, G. 2002, *Astronomy and Astrophysics*, 381, 524, doi: [10.1051/0004-6361:20011493](https://doi.org/10.1051/0004-6361:20011493)
- Weyant, A., Schafer, C., & Wood-Vasey, W. M. 2013, *The Astrophysical Journal*, 764, 116, doi: [10.1088/0004-637X/764/2/116](https://doi.org/10.1088/0004-637X/764/2/116)
- Wong, K. W. K., Contardo, G., & Ho, S. 2020, *Physical Review D*, 101, 123005, doi: [10.1103/PhysRevD.101.123005](https://doi.org/10.1103/PhysRevD.101.123005)
- York, D. G., Adelman, J., Anderson, Jr., J. E., et al. 2000, *The Astronomical Journal*, 120, 1579, doi: [10.1086/301513](https://doi.org/10.1086/301513)
- Zhang, K., Bloom, J. S., Gaudi, B. S., et al. 2021, doi: [10.3847/1538-3881/abf42e](https://doi.org/10.3847/1538-3881/abf42e)